Supporting Information

1. Molecular simulation

1.1. Model construction

The head and tail atoms of P(AA-*co*-VBA), PAA, and PEO repeating units were defined to construct a molecular chain with polymerization degree of 50. The molecular chain of P(AA-*co*-VBA) was simplified to PAA. The molecular chain of PAA and PEO is shown in the Figure S1a and b.

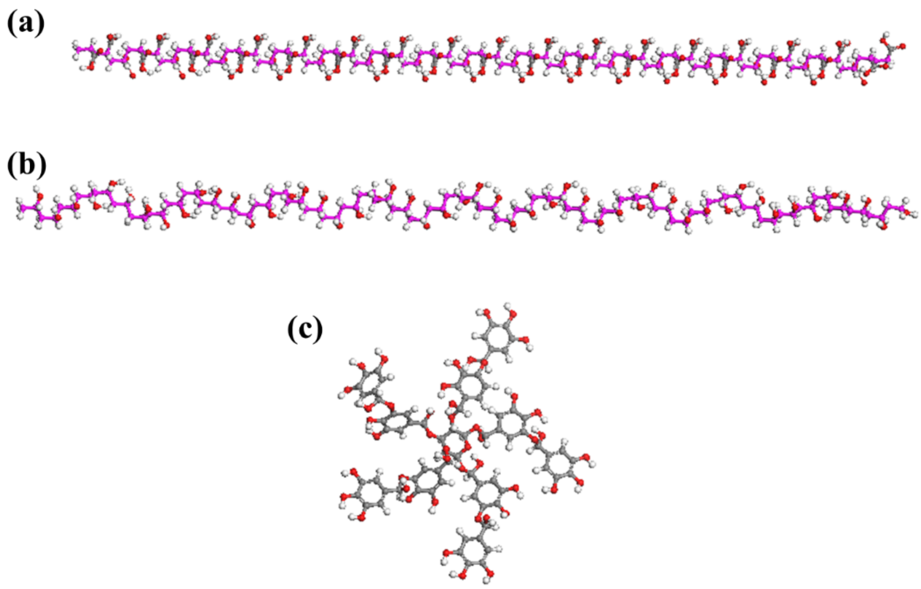

Figure S1. (a) Partial molecular chain model of P(AA-*co*-VBA), (b) partial molecular chain model of PEO, (c) molecular model of TA.

1.2. Energy optimization

Energy minimization is required for the polymer before further calculate. Energy minimization can eliminate unnecessary overlap of atoms and high energy conformation caused by unreasonable structure, and obtained conformation with the lowest molecular potential energy. Energy minimization uses smart Minimizer algorithm under Discover module to obtain the most stable conformation. After obtaining the most stable conformation, Amorphous Cell is constructed by Calculation in Amorphous Cell module. Amorphous cells are periodic cells, that is, periodic boundary conditions are applied in three directions. In addition to energy minimization, amorphous cells also need annealing to obtain the most stable structure with the lowest potential energy. Anneal in Forcite module is used for annealing treatment. The purpose of annealing is to allow amorphous cells to gain more energy to cross the potential barrier at high temperature, so that the molecular chain is sufficiently relaxed[1]. P(AA-*co*-VBA)/PEO/TA amorphous cells were constructed, and each cell contained 5 P(AA-*co*-VBA), 5 PEO and 1 TA molecular. And the model is optimized for energy shown in Figure S2a[2].

1.3. Molecular dynamics simulation

Dynamics in Forcite module was used for molecular Dynamics simulation. Andersen was used for pressure control and Berendsen constant temperature bath was used for temperature control. The integration method of Newton equation adopts velocity Verlet algorithm, and the integration time step is L fs. The electrostatic interaction was calculated using the Ewald method with an accuracy of 0.001kcal*mol^{-1}, and the hydrogen bond interaction was calculated using the Lennard-Jones function.

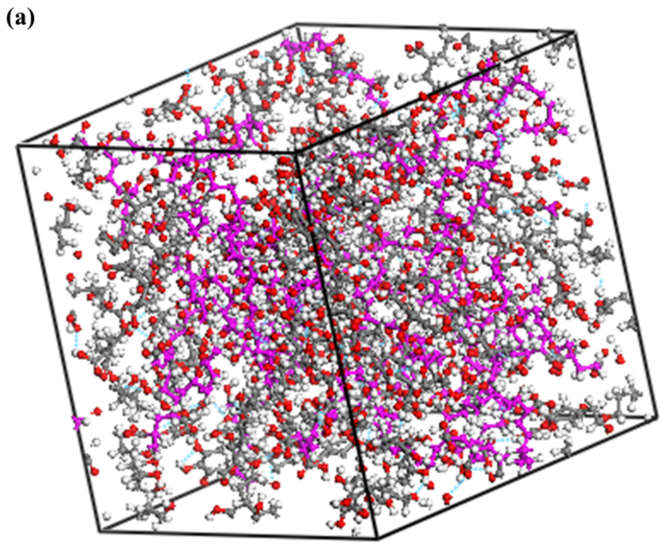

Figure S2. (a) Amorphous cells of P(AA-*co*-VBA)/PEO/TA.

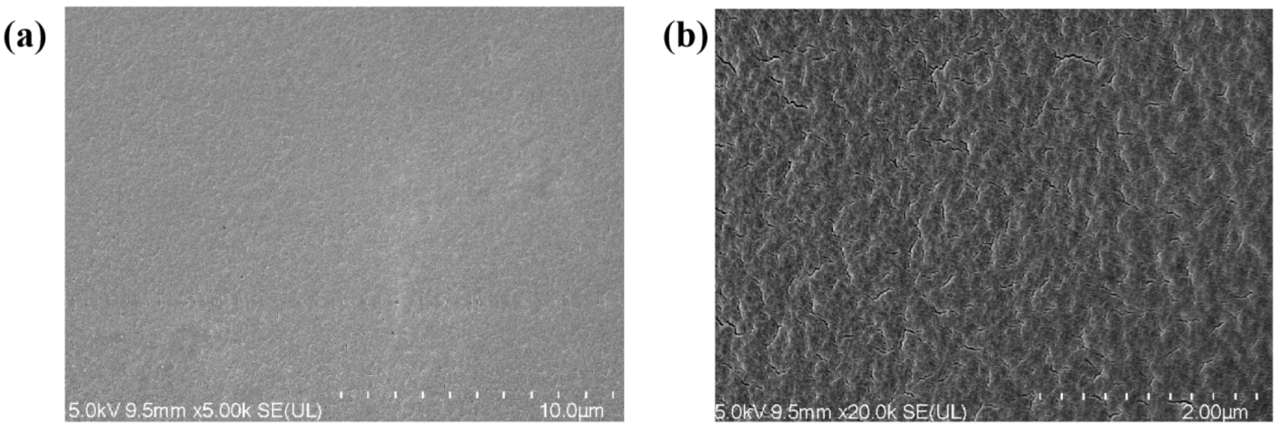

Figure S3**.** SEM image of PAVT (a and b).

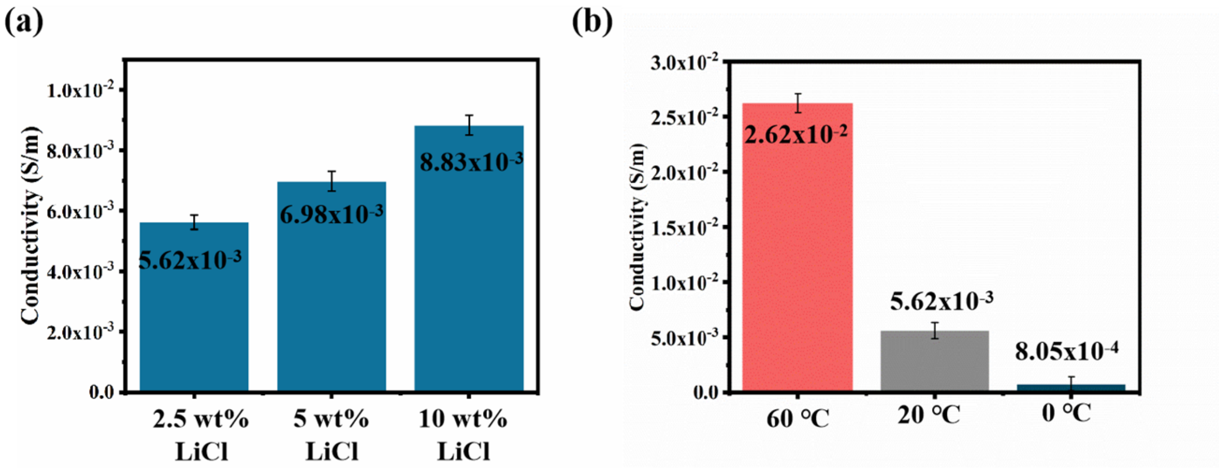

Figure S4. (a) The electrical conductivity of PAVT with different content of LiCl, and (b) electrical conductivity of PAVT with 2.5 wt% LiCl at different temperatures.

As shown in Figure S4a, with the increase of Li^+ ion concentration from 2.5 wt% to 10 wt%, the conductivity of PAVT increased from $5.62*10^{-3}$ S/m to $8.83*10^{-3}$ S/m.

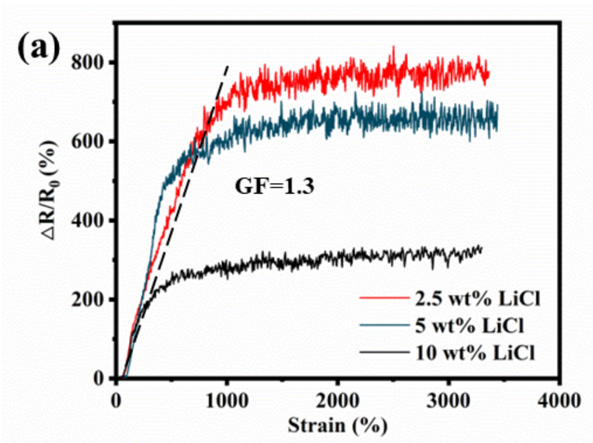

Figure S5. (a) Relative resistance change of the sensors based on PAVT of different LiCl loadings.

Under the action of electric field, Li^+ will undergo continuous complexation and dissociation process with the thermal movement of amorphous high elastic region chain segment, and Li^+ completes directional migration with the change of free volume caused by the movement of chain segment. When PAVT stretched over 1000%, the movement of the chain was limited and the resistance was not changing.

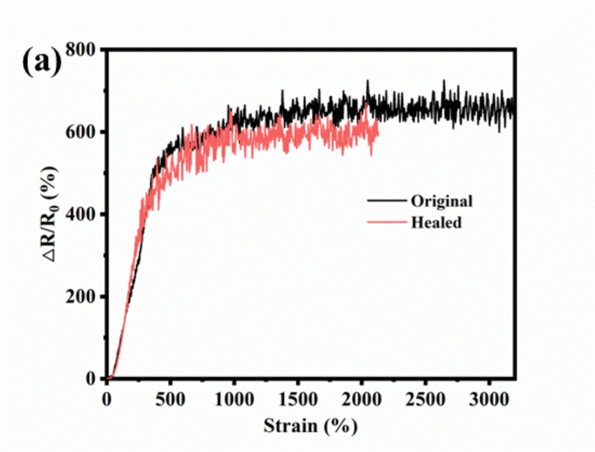

Figure S6. (a) Relative resistance change of original and 24 h healed sensors.

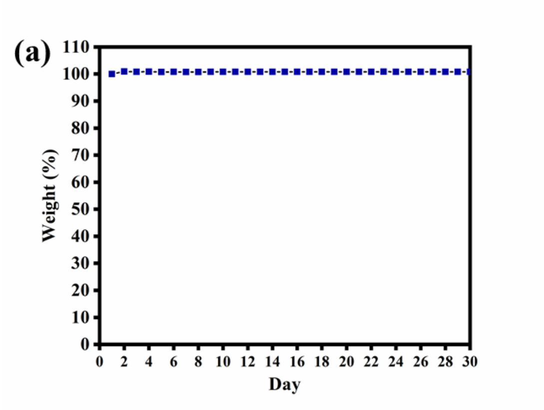

Figure S7. (a) Mass change of PAVT exposured to air during 30 days.

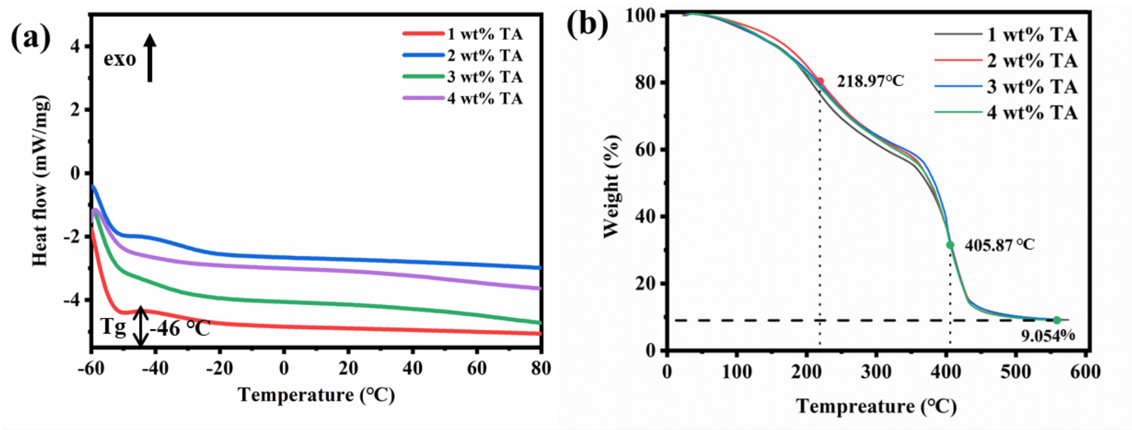

Figure S8. (a) The DSC and (b) TGA results of PAVT with different content of TA.

Table S1. Compositions of PAVT with different BIS content.

Samples	AA (g)	PEO (g)	TA (mg)	BIS (mg)	VBA (mg)	APS (mg)	LiCl (g)
1	2	2	120	0	20	20	0.1
2	2	2	120	4	20	20	0.1
3	2	2	120	20	20	20	0.1
4	2	2	120	40	20	20	0.1

Table S2. Compositions of PAVT with different TA content.

Samples	AA (g)	PEO (g)	TA (mg)	BIS (mg)	VBA (mg)	APS (mg)	LiCl (g)
1	2	2	40	4	20	20	0.1
2	2	2	80	4	20	20	0.1
3	2	2	120	4	20	20	0.1
4	2	2	160	4	20	20	0.1

Table S3. Compositions of PAVT with different LiCl content.

Samples	AA (g)	PEO (g)	TA (mg)	BIS (mg)	VBA (mg)	APS (mg)	LiCl (g)
1	2	2	120	4	20	20	0.1
2	2	2	120	4	20	20	0.2
3	2	2	120	4	20	20	0.4

Table S4. References show in Figure 3d.

Serial number	Reference
1	Jiaying Mo, Yuhang Dai, Chao Zhang et al. Design of ultra-stretchable, highly adhesive and self-healable hydrogels by tannic acid-enabled dynamic interactions Materials horizons, 2021.8,3409-3416
2	Xing Su, Yang Luo, Zhuoling Tian et al. Ctenophore-inspired hydrogels for efficient and repeatable underwater specific adhesion to biotic surfaces Materials Horizons, 2020.7.2651
3	Yujia Liang, Kaifang Wang, Jingjing Li et al. Low-Molecular-Weight Supramolecular-Polymer Double-Network Eutectogels for Self-Adhesive and Bidirectional Sensors Advanced Functional Materials 2021, 31, 2104963
4	Xiaoxuan Wu, Hui Liao, Di Ma et al. A wearable, self-adhesive, long-lastingly moist and healable epidermal sensor assembled from conductive MXene nanocomposites Journal of Materials Chemistry C, 2020, 8, 1788--1795
5	Zhiang Shao, Xiangming Hu, Weimin Cheng et al. Degradable self-adhesive epidermal sensors prepared from conductive nanocomposite hydrogel Nanoscale 2020, 12, 18771
6	Lei Chen, Zhaolong Wang, Ziheng Zhan et al. 3D printed super-anti-freezing

	self-adhesive human-machine interface Materials Today Physics 19 (2021) 100404
7	Rui Lv, Zhongwu Bei, Yuan Huang et al. Mussel-Inspired Flexible, Wearable, and Self-Adhesive Conductive Hydrogels for Strain Sensor Macromolecular Rapid Communications 2020, 41, 1900450
8	Jianyu Yin, Shenxin Pan, Lili Wu, et al. A self-adhesive wearable strain sensor based on a highly stretchable, tough, self-healing and ultra-sensitive ionic hydrogel Journal of Materials Chemistry C, 2020, 8, 17349--17364
9	Feixue Lu, Yaoyao Wang, Chao Wang, et al. Two-Dimensional Nanocellulose-Enhanced High-Strength, Self Adhesive, and Strain Sensitive Poly(acrylic acid) Hydrogels Fabricated by a Radical-Induced Strategy for a Skin Sensor ACS sustainable chemistry engineering 2020, 8, 3427-3436

Table S5. The equation obtained by fitting the curve in Figure 4b.

Function 1	y = Intercept + B1*x^1 + B2*x^2 + B3*x^3 + B4*x^4 + B5*x^5
Intercept	-0.05452 ± 0.35102
B1	-4.78686 ± 0.09726
B2	0.12141 ± 0.0077
B3	-0.00202 ± 2.29455E-4
B4	1.88384E-5 ± 2.86523E-6
B5	-7.04472E-8 ± 1.26752E-8
R-Square (COD)	0.99995

Table S6. The equation obtained by fitting the curve in Figure 4c.

Function 2	y = Intercept + B1*x^1 + B2*x^2 + B3*x^3 + B4*x^4 + B5*x^5+B6*x^6

Intercept	-0.48828 ± 0.02348
B1	0.02444 ± 0.0069
B2	-4.71387E-4 ± 6.26287E-4
B3	-3.03009E-6 ± 2.51578E-5
B4	2.61996E-7 ± 4.98833E-7
B5	-3.57165E-9 ± 4.78145E-9
B6	1.54763E-11 ± 1.76748E-11
R-Square (COD)	0.99969

References

1. A. Khot and B. M. Savoie, *Macromolecules*, 2021, **54**, 4889-4901.
2. Michael L. Klein and W. Shinoda, *SCIENCE*, 2008, **321**, 798-800.